Ore Geology Reviews 102 (2018) 195–203

Contents lists available at ScienceDirect

Ore Geology Reviews

journal homepage: www.elsevier.com/locate/oregeorev

On the origin of large type IIa gem diamonds

Sergei K. Simakov

LLC "ADAMANT", Harchenko 19-A-7H, St. Petersburg 194100, Russia

ARTICLE INFO

Keywords:
Diamonds
Kimberlites
Fluids
Mantle
Crust

ABSTRACT

The processes of formation of some diamond types still raise contentious issues, mainly on the origin of the largest diamond crystals recovered from kimberlites. These diamonds constitute less than 2% of worldwide resources and correspond to rare type IIa. They possess some peculiar features: (i) silicate and oxide inclusions are extremely rare, (ii) their $\delta^{13}C$ ranges from −17 to −21‰. The detailed estimation of the Premier pressure-temperature-oxygen fugacity parameters and the physic-chemical modeling of diamond growth-dissolution processes suggest that extra-large diamonds have multiple origins. Their formation may occur from lower mantle to crustal depths. Their main building-up takes place from fluids in the pegmatitic veins solidified along the contacts of kimberlite magma at a crustal depth. The model explains the main features of the largest kimberlitic diamonds, i.e. their great sizes, light $\delta^{13}C$ signatures, low nitrogen contents, high degree of resorption, absence of mantle-derived mineral inclusions and their occurrence in the form of rare isolated crystals in the host kimberlite.

1. Introduction

Diamond is recognized as an extraordinary recorder of astrophysical and geodynamic events, which extend from far reaches of space to the Earth's deep interior. Processes of diamond formation still raise contentious issues, principally on the origin of the largest diamond crystals (bigger than 100 carats) recovered from kimberlites. Most of these diamonds correspond to the rare type IIa. They constitute less than 2% of worldwide resources, and include the largest gemstone ever found, the Cullinan (3106 ct), extracted from the Premier kimberlite, as well as the famous alluvial stones from India such as the Koh-I-Noor. These large diamonds mainly occur in well-known South African kimberlite mines (e.g. Cullinan and Jagersfontein), in several Lesotho kimberlites, in particular at Letseng la Terai, Mothae and Kolo, in Botswana (AK6, now Karowe), Jwaneng, Orapa, in Canada, West Africa and India (Gurney and Helmstaedt, 2012; Moore, 2009, 2014).

Type II diamonds have extremely low nitrogen contents (N < 30 ppm) and consist from two groups: IIa and IIb. As revealed by (IR) spectroscopy (Custers, 1952; Collins, 1982) type IIa are B-free and type IIb contain B. They represent a number of discrete parageneses, grown under variable mantle conditions. Eclogitic, peridotitic, websteritic and ultra-deep inclusions are reported in them (Moore, 2009; Sobolev et al., 1969). Large type IIa gem diamonds have some distinctive features: (i) highly resorbed crystals, (ii) low $\delta^{13}C$, (iii) irregular shape, occasionally with poorly preserved dodecahedral faces, but lacking octahedral habit (Gurney and Helmstaedt, 2012). They also have extremely low nitrogen contents (N < 10 ppm), often below the detection limits of many analytical instruments (Gaillou et al., 2012). They represent a distinct, hitherto unrecognized paragenesis (Moore, 2009). The main purpose of this work is to propose a new model for the extra-large type IIa diamond formation, which does not consider all type II stones. Their $\delta^{13}C$ (‰) signature spreads from −0.5 to −34‰, with a mode in the range −17 to −21‰ and with peaks at −20, −31 and −3‰ (Banas et al., 2017; Milledge et al., 1983), which recovers with eclogitic (Cartigny, 2005), transitional zone (Cartigny et al., 2014) and macrodiamonds and nanodiamonds hosted in a serpentinite xenolith (Simakov et al., 2015) and lavas of Tolbachik volcano (Galimov et al., 2016; Karpov et al., 2014) (Fig. 1). Mantle-derived silicate and oxide inclusions are extremely rare; the commonly reported inclusions are graphite and sulfides only (Bowen et al., 2009). Large type IIa diamonds are found as isolated crystals in diamond-poor kimberlite sections, completely lacking small diamond crystals (Levinson et al., 1992).

Several observations argue for the existence of multiple sources of type II diamonds (Moore, 2009). Smith et al. (2016) propose that their formation occurs in a redox-sensitive metallic liquid phase in deep mantle eclogites, at a depth range of 360–750 km. The latter is inferred from the assemblage constituted of majoritic garnet, calcium silicate perovskite, and reduced volatiles in the inclusions of type II gem diamonds, whose sizes span from 5 carats to 40 carats only.

Smith et al. (2016) observe Fe-Ni-C-S melt inclusions in the studied type II diamonds, which are consistent with rare iron meteorite

E-mail address: simakov@ap1250.spb.edu.

https://doi.org/10.1016/j.oregeorev.2018.08.023
Received 21 June 2018; Received in revised form 14 August 2018; Accepted 20 August 2018
Available online 23 August 2018

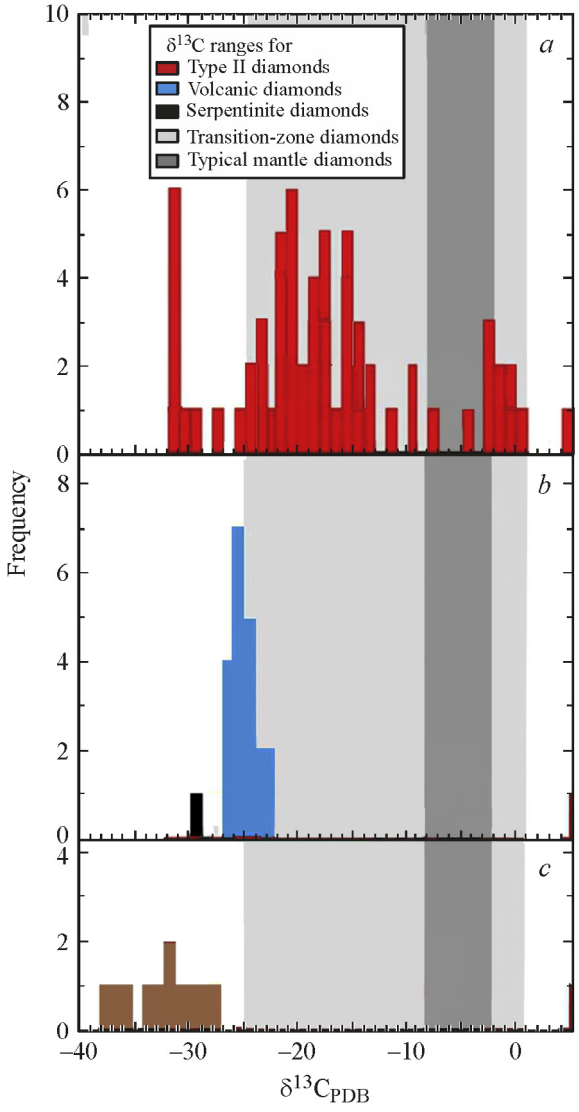

Fig. 1. Carbon isotope diagram of a) Type IIa diamonds, b) Volcanic and serpentinite micro- and nanodiamonds, c) volcanic methane. The data were taken from Banas et al. (2017); Cartigny et al. (2014), Etiope et al. (2013); Galimov et al. (2016); Karpov et al. (2014); Milledge et al. (1983), Simakov et al. (2015); Tappert et al. (2005).

paragenesis suggested by Arai (1986). Experimental growth of a high-quality diamond crystals demonstrates that the formation of diamond greater than 1000 carats would require the existence of iron bubbles of dozens centimeters in size (Borzdov et al., 2000; Sumiya et al., 2002). However, a few μm-sized Fe-Ni droplets only were observed in garnets from polycrystalline diamond aggregates (Jacob et al., 2004) hosted in abundant eclogite and peridotite xenoliths, representing the main parental rocks of diamonds in the mantle (Stachel and Harris, 2009). These μm-sized Fe-Ni droplets are compatible with the formation of μm-sized diamonds. The total absence of silicon (Table S2 in Smith et al., 2016) in these metal inclusions would hint at their formation at relatively low pressure (Takafuji and Hirose, 2005). Ultimately, the model cannot explain the absence of mantle-derived silicate and oxide inclusions in type IIa great gems and their lack of association with smaller size diamonds.

Furthermore, Smith et al. (2016) remark the low N content of type II diamonds, and tentatively explain this feature by the strong N partitioning into metal (Smith and Kopylova, 2014). However, the redox origin of these stones is incompatible with their low N amounts, since nitrogen and NH_3 quantities increase with redox in mantle fluids (Simakov, 1998; Sokol et al., 2017). This is proven by the fact that most reduced Premier eclogitic diamond parageneses are characterized by high nitrogen contents (Simakov, 2006), whereas type IIa stones are poor in nitrogen (Shigley, 2005).

In accordance with Moore (2009) the large irregular stones represent very late-crystallizing megacryst phases in pegmatitic veins, which crystallized from small volumes of kimberlite magma injected into fractures in the mantle wall rocks surrounding the main (unfractionated) parent kimberlite magma body. On the above considerations, type II diamonds can realistically form at P-T conditions corresponding to the region of the mantle solidus boundary, or lower (Simakov, 2018). Diamonds may form in the Earth's mantle by oxidation–reduction reactions involving carbonate or methane (Stachel and Luth, 2015). Since the Premier pipe contains the highest worldwide quantity of famous and most studied large gem diamonds (Gurney and Helmstaedt, 2012), it represents the ideal site to investigate the origin of these stones. Here, I propose a detailed P-T-fo_2 estimation for Premier pipe based on published data of electron microprobe (EMP) mineral analyses of the eclogitic diamond inclusions (Gurney et al., 1985; Korolev et al., 2018), and garnet and spinel peridotite xenoliths (Baptiste et al., 2012; De Hoog et al., 2010; Gregoire et al., 2005; Viljoen et al., 2009).

2. Methods of *P-T-fo*$_2$ estimation

For the garnet peridotite P-T estimation, garnet–orthopyroxene thermobarometers (Brey and Köhler, 1990; Harley, 1984) were used (Stachel and Luth, 2015). For the spinel peridotite P-T estimation, the olivine–spinel thermometer (O'Neill and Wall 1987) and the orthopyroxene barometer (Carswell, 1991) were applied (Nimis and Grutter, 2010). For the eclogite P-T estimation, garnet–clinopyroxene thermobarometers (Nakamura, 2009; Simakov, 2008) were employed.

The oxidation state can be estimated by redox reactions involving iron-bearing minerals. For spinel-bearing rocks, which usually originate at a depth range of 30–50 km, the oxythermobarometry calculations use the $FeFe_2O_4$ (magnetite) spinel component. Wood (1991) and Ballhaus et al. (1991) proposed the use of the spinel-orthopyroxene-olivine equilibrium reaction:

$$\underset{\text{orthopyroxene}}{6FeSiO_3} + \underset{\text{magnetite}}{2Fe_3O_4} = \underset{\text{olivine}}{6Fe_2SIO_4} + O_2 \quad \text{(I)}$$

For garnet-bearing rocks, which originate at depths between 50 and 220 km, the oxythermobarometry equilibria use the $Fe_3Fe_2Si_3O_{12}$ (skiagite) and $Ca_3Fe_2Si_3O_{12}$ (andradite) garnet components. Gudmundsson and Wood (1995) and Stagno et al. (2013) proposed the use of the reactions of the garnet-orthopyroxene-olivine equilibrium:

$$\underset{\text{garnet}}{2Fe_3Fe_2Si_3O_{12}} = \underset{\text{orthopyroxene}}{2FeSiO_3} + \underset{\text{olivine}}{4Fe_2SiO_4} + O_2 \quad \text{(II)}$$

$$\underset{\text{garnet}}{2Ca_3Fe_2Si_3O_{12}} + \underset{\text{garnet}}{2Mg_3Al_2Si_3O_{12}} + \underset{\text{orthopyroxene}}{4FeSiO_3} = \underset{\text{olivine}}{4Fe_2SiO_4} + \underset{\text{garnet}}{2Ca_3Al_2Si_3O_{12}} + \underset{\text{orthopyroxene}}{6MgSiO_3} + O_2 \quad \text{(III)}$$

For eclogitic parageneses, Simakov (2006) and Stagno et al. (2015) proposed the reactions of the garnet-clinopyroxene-silica equilibrium:

$$\underset{\text{garnet}}{2Ca_3Fe_2Si_3O_{12}} + \underset{\text{orthopyroxene}}{Fe_2Si_2O_6} + \underset{\text{Qtz(Coe)}}{4SiO_2} = \underset{\text{clinopyroxene}}{6CaFeSi_2O_6} + O_2 \quad \text{(IV)}$$

Ballhaus et al. (1991) have demonstrated that stoichiometric Fe^{3+} in spinel agrees well with ones measured by Mössbauer spectroscopy. The level of imprecision in Fe^{3+} determined from electron microprobe (EMP) analyses is related to the total Fe content, and increases in the order: spinel < garnet < clinopyroxene. Because ferric iron is low in garnet, the garnet barometers require a careful measurement of $Fe^{3+}/\Sigma Fe$. There are only two analytical methods commonly used to determine $Fe^{3+}/\Sigma Fe$ directly, Mössbauer spectroscopy, and wet

Table 1
Garnet-olivine-orthopyroxene and spinel-olivine-orthopyroxene parageneses used for P-T-fo_2 calculations. BK90 – Grt-Opx barometer of Brey and Köhler (1990) (stand. dev. ± 6.6 kbar), C91 – Opx barometer of Carswell (1991) (stand. dev. ± 4.9 kbar); H84 – Grt-Opx thermometer of Harley (1984) (stand. dev. ± 100 °C), NW87 – Ol–Sp thermometer of O'Neill and Wall (1987). % Fe^{3+}_{Sp} = 100*Fe^{3+}/(Fe^{3+} + Fe^{2+}), $_{\Delta}$lg(fo_2) – calculated values relative to QFM buffer by spinel-olivine-orthopyroxene barometer of Wood (1991) (stand. dev. ± 0.5 lg fo_2). Analyses for the calculations were taken from: De Hoog et al. (2010), Gregoire et al. (2005), Viljoen et al. (2009).

Sample	C91	NW87	BK90	H84	%Fe^{3+}_{Sp}	$_{\Delta}$ lg(fo_2)
Spinel lherzolites						
PR89-35	21	730			6.4	−2.2
PR90-21	25	853			6.0	−3.2
PR90-24	22	789			15.9	−0.9
PR90-4	24	715			7.2	−1.8
PR90-29	17	709			0.0	–
Garnet-spinel lherzolites						
RVD172			43.7	1120	22.24	−0.7
RVD184			33	937	0.8	−4.3
FB1325			18.3	747	20.7	−2.3

Table 2
Eclogite garnet-clynopyroxene parageneses separated for the P-T-fo_2calculations. (Si + Ti) – silica and titan content in garnet (in f.u.), % Fe^{3+}_{Grt} = 100*Fe^{3+}/(Fe^{3+} + Fe^{2+}), N09 – Grt-Cpx thermometers of Nakamura (2009) (stand. dev. ± 74 °C). S08 - Grt- Cpx barometer of Simakov (2008) (stand. dev. ± 4.6 kbar),$_{\Delta}$lg(fo_2) – calculated values relative to QFM buffer by the oxygen Grt-Cpx-Qtz barometer of Simakov (2006) with stand. dev. ± 0.8 lg fo_2. N, ppm – nitrogen content in the diamond in ppm by the data of Deines et al. (1989) and Korolev et al. (2018). Analyses for the calculations were taken from: Gurney et al. (1985) and Korolev et al. (2018).

Sample	S08	N09	(Si + Ti)$_{Grt}$	%Fe^{3+}_{Grt}	$_{\Delta}$ lg(fo_2)	N, ppm
P-3	58	1438	3.04	4.0	−4.9	618
P-18	68	1604	3.02	9.2	−3.8	142
P-35	44.5	1165	3.02	11.3	−1.3	175
P-37	68.5	1462	3.01	0	–	100
P-38	42	1134	3.01	1	−8.0	943
P-43	70	1472	3.01	0	–	123
P44	66.1	1444	3.01	6.5	−5.1	
P45	68.4	1594	3.02	6.2	−3.2	29
P46	46	1190	3.01	12.0	−1.3	118
P47	59.2	1409	3.03	1.9	−5.1	464
P65	70.5	1467	3.04	4.2	−4.3	503
P66	67	1370	3.01	4.7	−4.2	163
P103	52.3	1238	3.01	6.5	−3.6	496
P104	39	1063	3.01	11.4	−1.0	40
P105	71.5	1443	3.02	0	–	496
P106	57	1205	3.01	0	–	735
P109	54.5	1266	3.04	0.7	−8.0	789
P111	61.7	1464	3.01	0	–	1057
P113	50.7	1236	3.04	5.4	−3.0	318
P115	51	1243	3.02	11.6	−1.6	129
110	59.2	1462	3.00	0	–	87
139	62.2	1420	3.02	2.5	−5.2	250
164	50.5	1332	3.02	9.0	–	58
176	60	1460	3.005	12.0	–	283
308	64.4	1528	3.00	11.0	–	305
324	56	1452	3.00	10.3	–	252
355	63.5	1543	3.00	0	–	57

chemistry. It is a common practice to use the crystal chemistry of silicate phases analyzed by electron microprobe to calculate the Fe^{3+} of a mineral. A comparison of the Fe^{3+}/ΣFe values calculated by Schumacher model (1991) with those determined by Mössbauer techniques for mantle garnets shows the correlation between the error in garnet Fe^{3+}/ΣFe determination and Si and Si + Ti contents (Simakov, 2006). The lowest error lies in the range of 3.03 ± 0.02 f.u. (Si + Ti) and corresponds to ± 0.8 log units (Simakov, 2006).

3. Results and discussion

P-T-fo_2 parameters were calculated for eclogitic diamond inclusions and peridotite xenoliths from the Premier pipe. Calculated P-T parameters for peridotite xenoliths correspond to the range of 709–1310 °C in temperature and 17–59 kbar in pressure (Table 1; Fig. 2). For eclogitic diamond inclusions calculated temperatures range from 1063 to 1604 °C at pressures of 39–71 kbar (Table 2; Fig. 2). These computed temperatures are within the range of experimental calibration temperatures (800–1820 °C), where they are accurate to ± 74 °C (Nakamura, 2009). These estimated P-T values accord with previous estimations of the Premier peridotite xenoliths (Boyd et al., 1999; Baptiste et al., 2012; De Hoog et al., 2010; Viljoen et al., 2009) and eclogite diamond inclusions (Simakov, 2008; Korolev et al., 2018).

A major problem of fo_2 calculation for the peridotite xenoliths is that the considered literature data have low control on quality. For this reason, fo_2 values were estimated only for spinel and spinel-garnet peridotites using spinel–olivine-orthopyroxene oxygen barometer of Wood (1990). Calculated fo_2 values lie between the Iron-Wüstite (IW) and the Quartz-Fayalite-Magnetite (QFM) oxygen buffers (Fig. 3). For eclogitic diamond inclusions fo_2 values were estimated using garnet-clinopyroxene-silica oxygen barometer of Simakov (2006). Previously garnet–clinopyroxene pairs were chosen for the fo_2 calculations by the Si and Ti contents. Calculated fo_2 values lie on 3 orders lower IW and between IW and the Wüstite-Magnetite (WM) oxygen buffers (Fig. 3). The total oxygen fugacity mainly decreases from the oxidized lithosphere to the reduced asthenosphere (Fig. 3), hence peridotite reduction increases with increasing depth. Fluid compositions were estimated

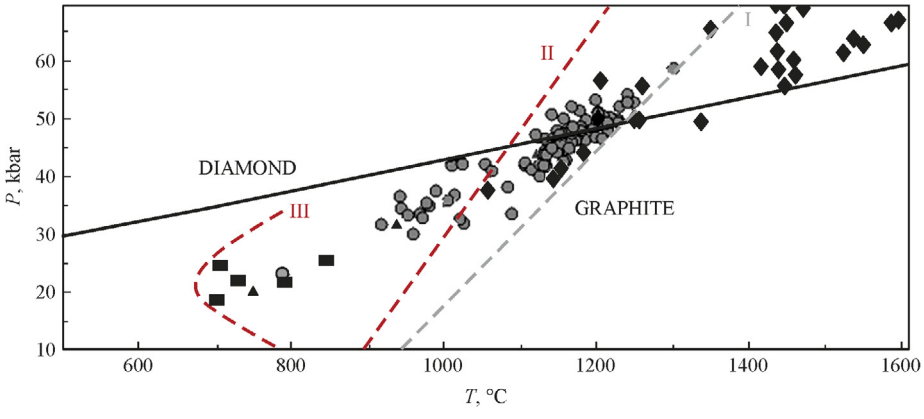

Fig. 2. P–T-fo_2 plot of the Premier garnet (●), garnet-spinel (▲) and spinel (■) peridotite xenoliths, (♦) eclogitic diamond inclusions. For the eclogitic diamond inclusions the P-T were estimated using the garnet–clinopyroxene thermobarometers of Nakamura (2009) and Simakov (2008). For the garnet peridotites the P-T were estimated from the garnet–orthopyroxene thermobarometers of Brey and Köhler (1990) and Harley (1984). For the spinel peridotites the P-T were estimated applying the olivine–spinel thermometer of O'Neill and Wall (1987) and orthopyroxene barometer of Carswell (1991). Solid line: diamond–graphite boundary (Bundy et al., 1961), dashed grey line: eutectic of Fe-C system (Nakajima et al., 2009), dashed red lines: lherzolite-water (Wyllie and Ryabchikov, 2000) (II) and websteritic (Mysen and Boettcher, 1976) (III) soliduses. The analyses for the calculations were taken from Baptiste et al. (2012), De Hoog et al. (2010), Gregoire et al. (2005), Gurney et al. (1985), Viljoen et al. (2009).

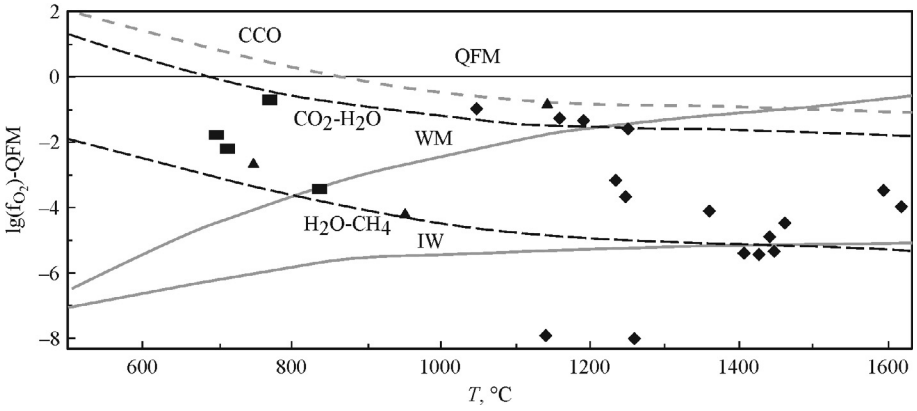

Fig. 3. T-fo_2 plot of the Premier eclogitic diamond inclusions estimated by using the garnet-clinopyroxene-silica oxygen barometer of Simakov (2006). For spinel and garnet-spinel peridotites spinel–olivine-orthopyroxene oxygen barometer of Wood (1991) was employed. Legend: QFM – Quartz-Fayalite-Magnetite, WM – Wüstite-Magnetite, IW – Iron-Wüstite oxygen buffers (Frost, 1991), CCO – is the oxygen fugacity calculated for the upper limit of carbon stability in C–H–O system corresponded to the reactions V and VI in accordance with Jakobsson and Oskarsson (1994) CO_2-H_2O and H_2O-CH_4 – boundaries of water-rich fluid. The analyses for the calculations were taken from the same sources reported in Fig. 2. The symbols are the same in Fig. 2.

as a function of P, T and fo_2 with the assumption that they were free carbon-saturated following the scheme described in Zhang and Duan (2010). The formation of large diamonds could be connected with C-O-H-N-S fluids (Taylor et al., 2003). The calculated peridotite fluids in the C–O–H system mainly correspond to a water-rich composition (Fig. 3). The water content smoothly decreases, and methane content increases in the calculated C–O–H system with depth.

From the calculated P-T, it follows that the upper boundary of the Premier eclogitic diamonds lies in the field of Fe-C melts, and the lower boundary of peridotite xenolith crystallization corresponds to the websterite solidus (Fig. 2). According to estimates by Stachel and Luth (2015), nearly 2% of world-diamond inclusions were formed at P-T conditions in the range of this solidus – at 630–680 °C and 30–34 kbar (Stachel and Luth, 2015, Fig. 2). It corresponds to the percent of large type IIa in the worldwide diamonds. From the C-O-H calculations, it is possible to conclude that equilibrated fluid compositions at the solidus boundary are rich in water. In the C–O–H fluid system, the upper limit of carbon stability in terms of fo_2 corresponds to the reactions of the CCO buffer:

$$CO_2 \rightarrow C + O_2 \quad (V)$$

$$CO \rightarrow C + 0.5O_2 \quad (VI)$$

The peridotite and eclogite assemblages lie at fo_2 below those of the CCO buffer (Fig. 3). In the mantle, however, the CCO buffer is of theoretical importance only. In the C–O–H system, diamond does not impose a lower fo_2 limit. One may place an arbitrary lower limit near an fo_2 defined by the equilibrium:

$$CH_4 + O_2 \rightarrow C + 2H_2O \quad (VII)$$

At this fo_2, methane changes into free carbon and water, and total atomic C content decreases in the fluid system. Below, when the partial pressures of CH_4 and H_2 exceed the partial pressures of CO_2 and CO, most free carbon transforms into methane. In this case, the total atomic C content increases in the fluid system. The least values of possible total atomic C content correspond to the maximum water content in the C-O-H fluid system and decrease with depth (Stachel and Luth, 2015). From the oxygen fugacity estimation for peridotite and eclogite, it derives that mantle diamond formation is mainly connected with water formation (Simakov, 1998, 2006; Stachel and Luth, 2015). The average composition of fluids extracted from African type IIa and Arkansas type II diamonds (Melton and Giardiny, 1974,1975) and experimental data of diamond syntheses (Sokol et al., 2009) confirm this conclusion.

P–T-fo_2 results obtained from eclogite inclusions in diamonds from the Premier pipe show a distinct kink in the oxygen-fugacity trajectory (Fig. 4). It is possible to distinguish two limbs in the trajectory. The first one is more reduced, and the oxygen fugacity increases with depth (limb I). It corresponds to diamonds with a high content of nitrogen. The second one is more oxidized, and the oxygen fugacity decreases with depth (limb II). It corresponds to diamonds with a relatively low content of nitrogen. From these calculations, it follows that the nitrogen content of diamonds increases with the lowering of the oxygen fugacity (Fig. 5), and that the diamond growth is mainly connected with the fluid O-H-N-C system.

The observed oxygen-fugacity trajectory can be explained by the possibility of the plume formation noted for the region of Bushveld igneous province (Korolev et al., 2018). Reduced plume melts could be intruded from deep levels of the asthenosphere to the lithosphere–asthenosphere boundary, or lower parts of the lithosphere, which contained subducted rocks and carbonates (Fig. 6). Plume melts could contain diamond seeds formed at great depth in the reduced asthenosphere. The nucleation of diamonds from metal-silicate melts is possible at this stage (Figs. 2 and 4, limb I). Further (upper part of limb I and limb II on Fig. 4), plumes could come in contact with lithosphere subducted rocks (Taylor and Green, 1989) (Fig. 6). Under the process of heating, the reaction Dol + Coe = liq + CO_2 would be crossed, releasing CO_2. Then the interaction of carbon dioxide with methane promotes the diamond formation:

$$CH_4 + CO_2 \rightarrow 2\,C + 2H_2O \quad (VIII)$$

The growth of diamonds in the field of WM buffer from fluids by the reaction (VIII) is possible at this stage. From these data, two main mechanisms of the Premier eclogite diamond formation can occur in the mantle: (1) crystallization of diamonds under very low fo_2 conditions from metallic melts; (2) diamond crystallization and growth under high fo_2 conditions in equilibrium with water-rich fluids. This scheme explains the presence of iron-nickel-carbon-sulfur melt, accompanied by a thin fluid layer of methane and majoritic garnet inclusions in type II diamonds (Smith et al., 2016). Additionally, it explains the presence of hydrous silicic fluid films in the Premier gem-quality diamonds (Nimis et al., 2016).

But this scheme couldn't explain the formation of extra-large Type IIa diamonds more than 100 carats with low $\delta^{13}C$ values and absence of lithospheric and astenospheric inclusions. Considering the rarity of silicate inclusions, extra-large diamonds could be formed at the P-T conditions near or below the websterite solidus. It is worth mentioning that $\delta^{13}C$ values of type IIa diamond are similar to those of volcanic methane and volcanic microdiamonds – Fig. 1. Phase relations in the C-O-H system and potential CH_4 generation during magma cooling at shallow depths were discussed in detail in Etiope and Sherwood Lollar (2013). Methane formation is possible at variations of P-T-fo_2 parameters from a water-saturated fluid at P-T lower than websterite solidus (Fig. 7). The formation of micron- and nano-sized diamonds could take place in fast-moving magmatic melts at pressure and temperature corresponding to graphite thermodynamic stability (Galimov, 1973; Galimov et al., 2016). Kimberlite magma could be pausing during uplift to surface (Giuliani et al., 2013, 2016). The so-called “polymict breccias”, which are generally thought to form in conduits during the ascent of kimberlite magmas were described in kimberlites of the Bultfontein

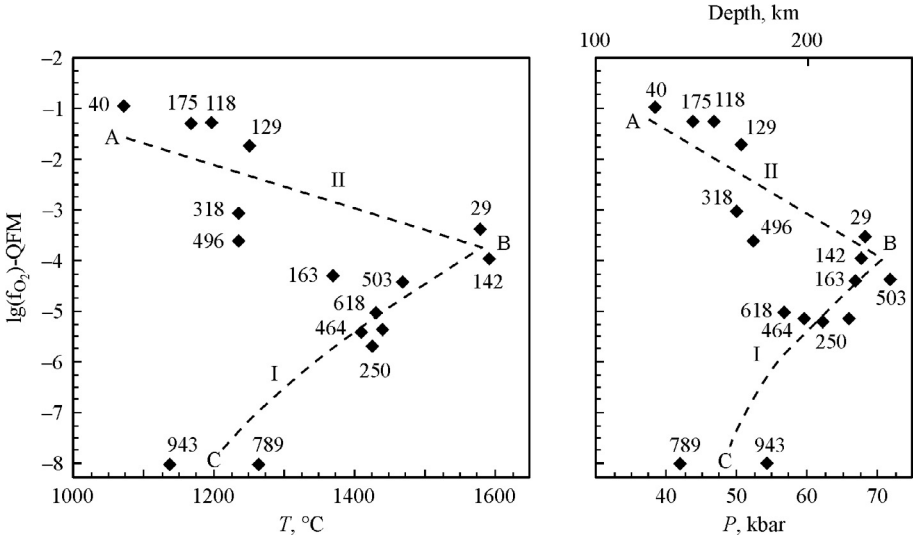

Fig. 4. T-fo_2 and P-fo_2 plots for the Premier eclogitic diamond inclusions based on data of Figs. 2 and 3. Data on nitrogen content of Deines et al. (1989) and Korolev et al. (2018) in ppm is plotted.

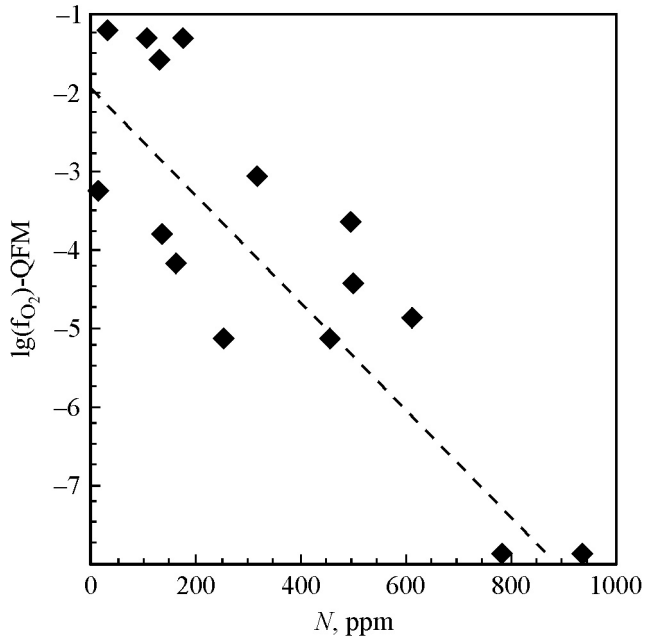

Fig. 5. The relationship between calculated fo_2 and nitrogen content (in ppm) for the Premier eclogitic diamonds.

Dumps (Kimberley, South Africa) and Lac de Gras (Slave Craton, Canada) (Bussweiler et al., 2018; Giuliani et al., 2013, 2014, 2016). These breccias include megacrysts carried up from great depths. The compositions of low-Cr phlogopite macrocryst rims from the Bultfontein and other kimberlites shows that these rims crystallized from the kimberlite magma upon emplacement in the upper crust (Beard et al., 2000; Downes et al., 2006). As a result, Giuliani et al. (2016) came to the conclusion that kimberlite magmas may only reach the surface by ascent through a pathway created by multiple magma pulses that metasomatise the conduit. The calculated P-T values for Cr-diopsides megacrysts of heavy-mineral concentrates from the "Big Hole" (Kimberley, South Africa) (Simakov, 2008), for garnet megacrysts from kimberlitic bodies of Northern Alberta (Simakov, 2012) and from heavy-mineral concentrates from Kaapwal, Montana and Daldyn (Ryan et al., 1996) confirm that they equilibrated and at a shallow depth. This inference implies that a kimberlite magma may stop during its upraise to shallower levels. In addition, the widespread presence of spinel-facies peridotite xenoliths in the Premier pipe (e.g., Khar'kiv et al., 1998), and that of upper overlaps in the Orapa (Field et al., 1995) and the Premier (Khar'kiv et al., 1998) pipes further support the "pausing" of kimberlite magmas. As a result, small magma volumes with mantle xenoliths and diamonds were injected into a fracture network, forming pegmatitic veins at a crustal level (Fig. 8).

Moreover, diamond growth on the existing mantle diamond seeds is possible from fluids at P-T parameters close to the diamond-graphite stability curve, during magma crystallization and the pegmatitic vein formation. Evidence of this process can be seen in the Nurbinskaya pipe, where metasomatic events occurred at the boundary of the hosted kimberlites and intruded trap intrusion (Khar'kiv et al., 1998). Spetsius et al. (2017) report a multistage diamond growth from parental mantle-related fluids with a crustal contribution of metasomatic reactions, which follows the introduction of lighter crustal carbon to initial mantle fluids. Distribution of diamond crystals within the products of kelyphite rims around garnet, as well as along general zones of partial melting indicate the origin of the diamonds on the late-stage of metasomatic events (Spetsius et al., 2008). Formation of either methane or free carbon in the C-O-H system depends upon the P-T-fo_2 parameters. From Fig. 7 it follows that methane could be formed from free carbon and water under decreasing temperature, pressure and oxygen fugacity. On the other hand, free carbon formation is favored by increasing temperature, pressure and fo_2 values.

The problem of the nitrogen presence in the upper mantle and kimberlite processes was discussed in several papers (e.g. Cartigny, 2005; Sobolev et al., 1966; Simakov, 1998, 2006; Stachel and Harris, 2009; Kaminsky and Wirth, 2017). I considered the reaction of the interaction of nitrogen with methane as another possible reaction responsible for the diamond formation process (Simakov, 1983, 1998):

$$N_2 + 1.5CH_4 \rightarrow 1.5C + 2NH_3 \quad \text{(IX)}$$

Sobolev et al. (1966) proposed that nitrogen was included in the diamond structure at a deep-seated stage of mantle degassing, e. g. included in the reaction:

$$NH_3 \rightarrow N^{3+} + 3H^- \quad \text{(X)}$$

NH_3 formation and its decomposition to H^- and N^{3+} decrease at decreasing temperature. The calculations in C-O-H-N system show that ammonia concentration must be inversely proportional to H_2O and CO_2 (Simakov, 2006). This agrees with the tendency of the nitrogen content of the Premier diamonds to decrease with increasing oxygen fugacity

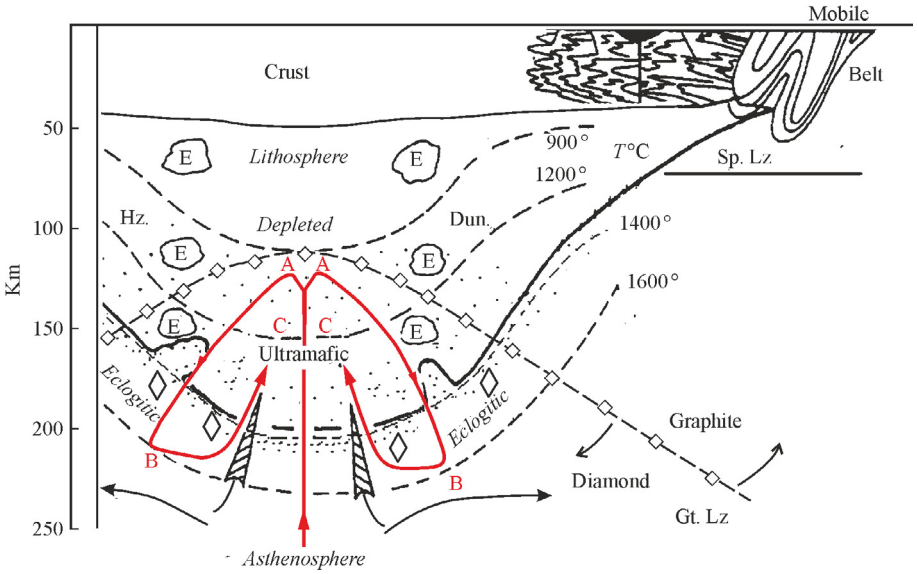

Fig. 6. Scheme of plume formation (red lines) in accordance with model of an Archean craton structure (Haggerty, 1999) and Premier P-T-fo_2trajectories (see Fig. 4). Legend: E – eclogite xenoliths, Sp.Lz. – spinel lherzolites, Gt.Lz. – garnet lherzolite, Dun. – dunites, Hz. – harzburgites, ◊ – diamonds, A,B, C – correspond to Fig. 4. (For interpretation of the references to colour in this figure legend, the reader is referred to the web version of this article.)

(Fig. 5). In natural diamonds the contents of nitrogen and hydrogen lower from the core to the rime (Kaminsky and Khachatryan, 2004; Griffin et al., 1995), which corresponds to decreasing decomposition of NH_3 to H^- and N^{3+} (reaction X) at declining temperature. In accordance with reaction (IX), NH_3 content in the fluid decreases with decreasing N_2 and CH_4 contents. Nitrogen, NH_3 and methane contents are increasing with depth (Simakov, 1998; Sokol et al., 2017). Major reservoirs of nitrogen should be expected in the core and in the lowermost mantle (Kaminsky and Wirth, 2017). From it follows that at the final stage of kimberlitic magma formation fluids are enriched in H_2O and CO_2 and depleted in nitrogen and ammonia. From the above premises, it follows that low nitrogen content of type IIa diamonds

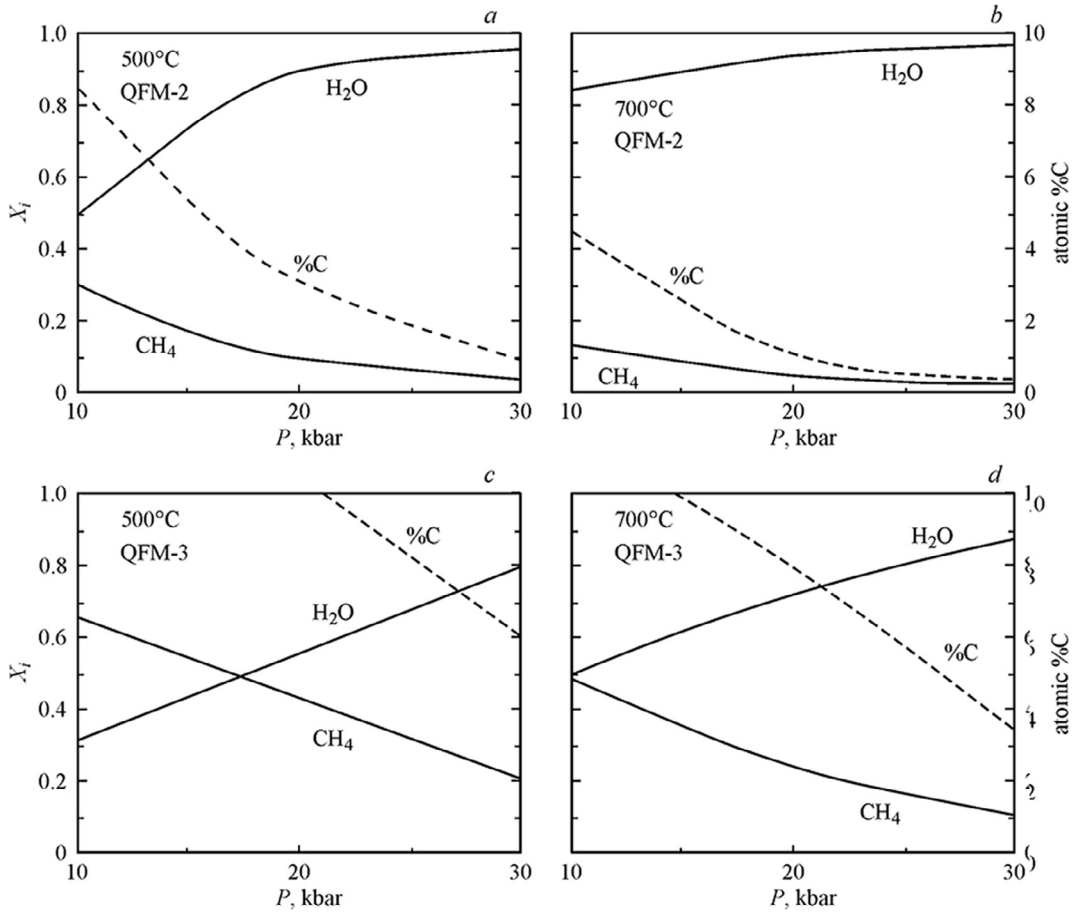

Fig. 7. Changes in the carbon content of diamond-saturated fluid with oxygen fugacity, pressure and temperature variations. Solid lines – molar parts of the main components of the C–H–O fluid system, dashed line – atomic percent in the fluid.

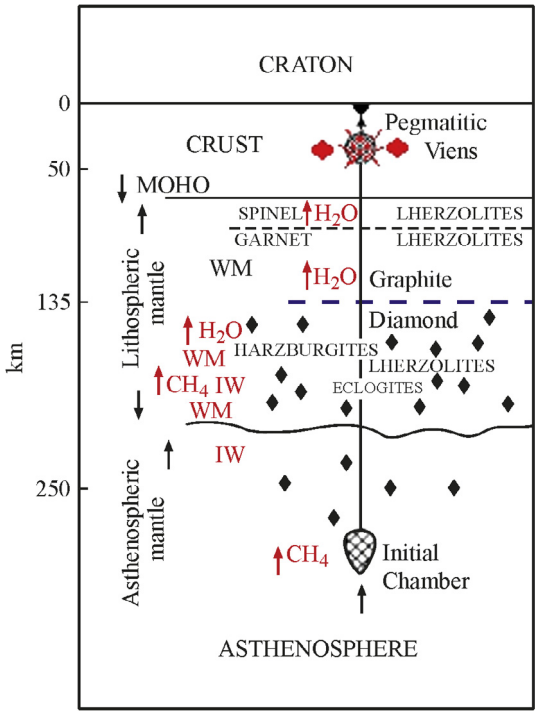

Fig. 8. Hypothetical cross-section of lithosphere structure under the Premier pipe in accordance with models of an Archean craton structure (Haggerty, 1999; Mitchell, 1991). Xenolith horizons are listed on the basis of the calculated P-T-fo_2 parameters, upper dashed line corresponds to spinel lherzolite – garnet lherzolite boundary, lower – to thermodynamic graphite-diamond boundary. Legend: ♦ – type I diamonds, red ⬡ – giant type IIa diamonds. (For interpretation of the references to colour in this figure legend, the reader is referred to the web version of this article.)

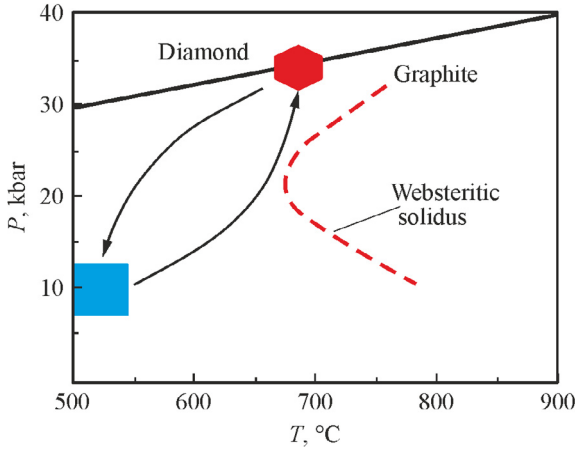

Fig. 9. Scheme of giant type IIa (red region) and volcanic methane (blue region) formations in accordance with variations of carbon content in diamond-saturated fluid from pressure (see Fig. 7). (For interpretation of the references to colour in this figure legend, the reader is referred to the web version of this article.)

indicates their origin at shallow depths.

As a result, it is possible to conclude that accidental variations of P-T-fo_2 conditions and fluid compositions in the system cause diamond growth-dissolution processes, and hence resorption of the diamond crystals. Such resorption follows the gradual building-up of large diamond stones and dissolution of small ones during cyclical growth-dissolution processes (Zhao et al., 1997). At the injection of magma into a fracture network at a crustal depth, the pressure and temperature of the fluid decrease. It follows to the small diamond and crustal terrestrial carbon dissolution in the water-rich fluid and volcanic methane formation (Fig. 9). Furthermore, at the presence of upper overlaps the flush of mantle fluids (Field et al., 1995) leads to the pressure and temperature increase up to the diamond thermodynamic stability. It follows to the gradual building-up of large diamond stones (Fig. 9). On the above grounds, diamond growth from fluid increases during the final stages of kimberlitic magma crystallization.

4. Conclusions

The results and considerations reported here deal with the problem of the largest sized natural diamond formation. In accordance with the presented model, extra-large type IIa diamonds have multiple origins. Their formation could be extended from lower mantle to crustal depths. Their main building-up takes place in the pegmatitic veins solidified along the contacts of kimberlite magma and crustal rocks, during the emplacement of the kimberlite magmas at a crustal depth. My results confirm that extra-large type IIa diamonds can form during the late stage of kimberlitic magma crystallization in the Earth's crust. Growth-dissolution processes of carbon in the fluid are followed by gradual building-up of large diamond stones on mantle seed crystals at this stage. It explains the main features of extra-large diamonds: their great sizes, integrity, light $\delta^{13}C$ signatures, low nitrogen contents, the high degree of resorption, the absence of mantle-derived silicate and oxide inclusions in them and non-association with small diamonds.

Acknowledgements

I wish to thank A. Moore, F. Manuella, G. Bulanova, T. Gerya, K. Kiseeva, P. Nimis, Y. Palyanov, C. Smith, N. Sobolev and A. Sokol for their stimulating discussions, comments and help and also F. Pirajno and the Reviewers for their careful editorial handling and constructive suggestions which helped me to improve the manuscript.

References

Arai, Sh., 1986. "Iron meteorite paragenesis", a new group of mineral inclusions in diamond. Neues Jahrbuch für Mineralogie 10, 463–466.
Ballhaus, C., Berry, R.F., Green, D.H., 1991. High pressure experimental calibration of the olivine–orthopyroxene–spinel oxygen geobarometer: implications for the oxidation state of the upper mantle. Contrib. Mineral. Petrol. 107, 27–40.
Banas, A., Stachel, T., Stern, R.A., Allan, A., Freeman, N., 2017. Can microdiamonds be used to predict the distribution of large Type IIa macrodiamonds? 11th International Kimberlite Conference. Extended Abstract 11IKC-4891.
Baptiste, V., Tomimasi, A., Demouchy, S., 2012. Deformation and hydration of the lithospheric mantle beneath the Kaapvaal craton, South Africa. Lithos 149, 31–50.
Beard, A.D., Downes, H., Hegner, E., Sablukov, S.M., 2000. Geochemistry andmineralogy of kimberlites from the Arkhangelsk Region, NW Russia: evidence for transitional kimberlite magma types. Lithos 51, 47–73.
Borzdov, Yu.M., Sokol, A.G., Pal'yanov, Yu.N., Khokhryakov, A.F., Sobolev, N.V., 2000. Growth of synthetic diamond monocrystals weighing up to six carats and perspectives of their application. Dokl. Earth Sci. 374, 1113–1115.
Boyd, F.R., Pearson, D.G., Mertzman, S.A., 1999. Spinel-facies Peridotites from the Kaapvaal root. In: Gurney, J.J., Gurney, J.L., Pascoe, M.D., Richardson, S.H. (Eds.), Proceedings of the VIIth International Kimberlite Conference. Cape Town, vol. 1, pp. 40–48.
Bowen, D.C., Ferraris, R.D., Palmer, C.E., Ward, J.D., 2009. On the unusual characteristics of the diamonds from the Letsent-la-terai kimberlites, Lesotho. Lithos 112S, 767–774.
Brey, G.P., Köhler, T., 1990. Geothermobarometry in four-phase lherzolites II. New thermobarometers, and practical assessment of existing thermobarometers. J. Petrol. 31, 1353–1378.
Bundy, F.R., Bovenkerk, H.P., Strong, H.M., Wentorf, R.H.J., 1961. Diamond–graphite equilibrium line from growth and graphitization of diamond. J. Chem. Phys. 35, 383–391.
Bussweiler, Y., Pearson, D.G., Stachel, T., Kjarsgaard, B.A., 2018. Cr-rich megacrysts of clinopyroxene and garnet from Lac de Gras kimberlites, Slave Craton, Canada – implications for the origin of clinopyroxene and garnet in cratonic lherzolites. Miner Petrol (https://doi.org/10.1007/s00710-018-0599-2).
Carswell, D.A., 1991. The garnet-orthopyroxene Al barometer: problematic application to natural garnet lherzolite assemblages. Mineral. Mag. 55, 19–31.
Cartigny, P., 2005. Stable isotopes and the origin of diamond. Elements 1, 79–84.
Cartigny, P., Palot, M., Thomassot, E., Jeff, W., Harris, J.W., 2014. Diamond formation: a stable isotope perspective. Annu. Rev. Earth Planet. Sci. 42, 699–732.

Collins, A.T., 1982. Colour centers in diamond. J. Gemmol. 18, 37–75.
Custers, J.F.H., 1952. Unusual phosphorescence of a diamond. Physica 18, 489–493.
De Hoog, J.C.M., Gall, L., Cornell, D.H., 2010. Trace element geochemistry of mantle olivine and application to mantle petrogenesis and geothermobarometry. Chem. Geol. 270, 196–215.
Deines, P., Harris, J.W., Spear, P.M., Gurney, J.J., 1989. Nitrogen and C content of Finsh and Premier diamonds and their implications. Geochim. Cosmochim. Acta 53, 1367–1378.
Downes, P.J., Wartho, J.-A., Griffin, B.J., 2006. Magmatic evolution and ascent history of the Aries Micaceous kimberlite, Central Kimberley Basin, Western Australia: evidence from zoned phlogopite phenocrysts, and UV laser 40Ar/39Ar analysis of phlogopitebiotite. J. Petrol. 47, 1751–1783.
Etiope, G., Tsikouras, B., Kordella, S., Ifandi, E., Christodoulou, D., Papatheodorou, G., 2013. Methane flux and origin in the Othrys ophiolite hyperalkaline springs, Greece. Chem. Geol. 347, 161–174.
Etiope, G., Sherwood Lollar, B.S., 2013. Abiotic methane on Earth. Rev. Geophys. 51, 1–24.
Field, M., Gibson, G.J., Wilkes, T.A., Gababotse, G., Khujve, P., 1995. The geology of the Orapa A/K1 kimberlite, Botswana. Futher insight into the emplacement of kimberlite pipes. 6th International Kimberlite Conference. Extended Abstracts. Novosibirsk. 1995. p.155–157.
Frost, B.R., 1991. Introduction to oxygen fugacity and its petrological importance. Rev. Mineral. Geochem. 25, 1–9.
Gaillou, E., Post, J.E., Rost, D., Butler, J.E., 2012. Boron in natural type IIb diamonds: chemical and spectroscopic measurements. Am. Mineral. 97, 1–18.
Galimov, E.M., 1973. Possibility of natural diamond synthesis under conditions of cavitation, occurring in a fast-moving magmatic melt. Nature 243, 389–392.
Galimov, E.M., Sevastyanov, V.S., Karpov, G.A., Shilobreeva, S.N., Maximov, A.P., 2016. Microcrystalline diamonds in oceanic lithosphere and their possible origin. Dokl. Earth Sci. 469, 70–72.
Giuliani, A., Kamenetsky, V.S., Kendrick, M.A., Phillips, D., Wyatt, B.A., Maas, R., 2013. Oxide, sulphide and carbonate minerals in a mantle polymict breccia: metasomatism by proto-kimberlite magmas, and relationship to the kimberlite megacrystic suite. Chem. Geol. 353, 4–18.
Giuliani, A., Phillips, D., Kamenetsky, V.S., Kendrick, M.A., Wyatt, B.A., Goemann, K., Hutchinson, G., 2014. Petrogenesis of Mantle Polymict Breccias: insights into Mantle Processes Coeval with Kimberlite Magmatism. J. Petrol. 55, 831–858.
Giuliani, A., Phillips, D., Kamenetsky, V.S., Goemann, K., 2016. Constraints on kimberlite ascent mechanisms revealed by phlogopite compositions in kimberlites and mantle xenoliths. Lithos 240–243, 189–201.
Gregoire, M., Tinguely, C., Bell, D.R., le Roex, A.P., 2005. Spinel lherzolite xenoliths from the Premier kimberlite (Kaapvaal craton, South Africa): nature and evolution of the shallow upper mantle beneath the Bushveld complex. Lithos 84, 185–205.
Griffin, B.J., Bulanova, G.P., Taylor, W.R., 1995. CL and FTIR mapping of nitrogen content and hydrogen distribution in a diamond from the Mir pipe – constrains of growth history. 6th International Kimberlite Conference, Novosibirsk, Extended Abstract, pp. 191–193.
Gudmundsson, G., Wood, B.J., 1995. Experimental tests of garnet peridotite oxygen barometry. Contrib. Miner. Petrol. 119, 56–67.
Gurney, J.J., Helmstaedt, H.H., 2012. Type IIA diamonds and their enhanced economic significance. 10th International Kimberlite Conference, Bangalore, India, Extended Abstracts, Unpaginated.
Gurney, J.J., Harris, I.W., Rickard, R.S., Moore, R.O., 1985. Inclusions in premier mine diamonds. Trans. Geol. Soc. South Africa 88, 301–310.
Haggerty, S.E., 1999. A diamond trilogy: superplumes, supercontinents, and supernovae. Science 285, 851–860.
Harley, S.L., 1984. An experimental study of the partitioning of iron and magnesium between garnet and orthopyroxene. Contrib. Miner. Petrol. 86, 359–373.
Jacob, D.E., Kronz, A., Viljoen, K.S., 2004. Cohenite, native iron and troilite inclusions in garnets from polycrystalline diamond aggregates. Contrib. Miner. Petrol. 146, 566–576.
Jakobsson, S., Oskarsson, N., 1994. The system C-O in equilibrium with graphite at high pressure and temperature: an experimental study. Geochim. Cosmochim. Acta 58, 9–17.
Kaminsky, F.V., Khachatryan, G.K., 2004. The relationship between the distribution of nitrogen impurity centers in diamond crystals and their internal structure and mechanism of growth. Lithos 77, 255–271.
Kaminsky, F.V., Wirth, R., 2017. Nitrides and carbonitrides from the lowermost mantle and their importance in the search for Earth's "lost" nitrogen. Am. Mineral. 102, 1667–1676.
Karpov, G.A., Silaev, V.I., Anikin, L.P., Rakin, V.I., Vasil'ev, E.G., Filatov, S.K., Petrovskii, V.A., Flerov, G.B., 2014. Diamonds and accessory minerals in products of the 2012–2013 Tolbachik Fissure Eruption. J. Volcanol. Seismolog. 8, 323–339.
Khar'kiv, A.D., Zinchuk, N.N., Kryuchikov, A.I., 1998. Diamond Primary Deposits of the World. Nedra, Moscow, pp. 555p.
Korolev, N.M., Kopylova, M., Bussweiler, Y., Pearson, D.G., Gurney, J., Davidson, J., 2018. The uniquely high-temperature character of Cullinan diamonds: a signature of the Bushveld mantle plume? Lithos 304–307, 362–373.
Levinson, A.A., Gurney, J.J., Kirkley, M.B., 1992. Diamond sources and production: past, present, and future. Gems Gemol. 28, 234–254.
Melton, C.E., Giardiny, A.A., 1974. The composition and significance of gas released from natural diamonds from Africa and Brazil. Am. Mineral. 59, 775–782.
Melton, C.E., Giardiny, A.A., 1975. Experimental results and a theoretical interpretation of gaseous inclusions in Arkansas natural diamonds. Am. Mineral. 60, 413–417.
Milledge, H.J., Mendelsohn, M.J., Seal, M., Rouse, J.E., Swart, P.K., Pillinger, C.T., 1983. Carbon isotopic variation in spectral Type II Diamonds. Nature 303, 791–792.
Mitchell, R.H., 1991. Kimberlites and lamproites: primary sources of diamond. Geosci. Can. 18, 1–16.
Moore, A.E., 2014. The origin of large irregular gem-quality type II diamonds and the rarity of blue type IIB varieties. S. Afr. J. Geol. 117, 219–236.
Moore, A.E., 2009. Type II diamonds: Flamboyant Megacrysts? S. Afr. J. Geol. 112, 23–38.
Mysen, B., Boettcher, A.L., 1976. Melting of a hydrous mantle: III. Phase relations of garnet websterite + H2O at high pressures and temperatures. J. Petrol. 17, 1–14.
Nakajima, Y., Takahashi, E., Suzuki, T., Funakoshi, K-i, 2009. «Carbon in the core» revisited. Phys. Earth Planet. Int. 174, 202–211.
Nakamura, D., 2009. A new formulation of garnet-clinopyroxene geothermometer based on accumulation and statistical analysis of a large experimental data set. J. Metamorph. Geol. 27, 495–508.
Nimis, P., Grutter, H., 2010. Internally consistent geothermometers for garnet peridotites and pyroxenites. Contrib. Miner. Petrol. 159, 411–427.
Nimis, P., Alvaro, M., Nestola, F., Angel, R.J., Marquardt, K., Rustioni, G., Harris, J.W., Marone, F., 2016. First evidence of hydrous silicic fluid films around solid inclusions in gem-quality diamonds. Lithos 260, 384–389.
O'Neill, H.St.C., Wall, V.J., 1987. The olivine-orthopyroxene-spinel oxygen geobarometer, the nickel precipitation curve, and the oxygen fugacity of the Earth's upper mantle. J. Petrol. 28, 1169–1191.
Ryan, C.G., Griffin, W.L., Pearson, N.J., 1996. Garnet geotherms: pressure-temperature data from Cr-pyrope garnet xenocrysts in volcanic rocks. J. Geophys. Res. 101, 5611–5625.
Shigley, J.E., 2005. High-pressure-high-temperature treatment of gem diamonds. Elements 1, 101–104.
Schumacher, J.C., 1991. Empirical ferric iron corrections: necessity, assumption, and effects on selected geothermobarometers. Mineral. Mag. 55, 3–18.
Simakov, S.K., 1983. Formation of carbon in the mantle fluid during interaction of nitrogen with methane. Doklady Akademi Nauk SSSR 268, 206–210 (in Russian).
Simakov, S.K., 1998. Redox state of earth's upper mantle peridotites under the ancient cratons and it connection with diamond genesis. Geochim. Cosmica Acta 62, 1811–1820.
Simakov, S.K., 2006. Redox state of eclogites and peridotites from sub-cratonic upper mantle and a connection with diamond genesis. Contrib. Miner. Petrol. 151, 282–296.
Simakov, S.K., 2008. Garnet-clinopyroxene and clinopyroxene geothermobarometry of deep mantle and crust eclogites and peridotites. Lithos 106, 125–136.
Simakov, S.K., 2012. New garnet thermometer for mantle peridotites and estimation of the diamond potential on its basis. Dokl. Earth Sci. 445, 1003–1005.
Simakov, S.K., 2018. Type IIa diamond formation. Dokl. Earth Sci. 482, 125–130 (accepted).
Simakov, S.K., Kouchi, A., Mel'nik, N.N., Scribano, V., Kimura, Y., Hama, T., Suzuki, N., Saito, H., Yoshizawa, T., 2015. Nanodiamond finding in the Hyblean shallow mantle xenoliths. Sci. Rep. 5, 10765. https://doi.org/10.1038/srep10765.
Smith, E.M., Kopylova, M.G., 2014. Implications of metallic iron for diamonds and nitrogen in the sublithospheric mantle. Can. J. Earth Sci. 51, 510–516.
Smith, E.M., Shirey, S.B., Nestola, F., Bullock, E.S., Wang, J., Richardson, S.H., Wang, W., 2016. Large gem diamonds from metallic liquid in Earth's deep mantle. Science 354, 1403–1405.
Sobolev, E.V., Lenskaya, S.V., Lisoyvan, V.I., 1966. Some physical properties of diamonds of Yakutian eclogite. Doklady Akademi Nauk SSSR 168, 1151–1153 (in Russian).
Sobolev, N.V., Lavrent'ev, Yu.G., Pospelova, L.N., Sobolev, E.V., 1969. Chromium pyropes from Yakutian diamonds. Doklady Akademii Nauk SSSR 189, 162–165 (in Russian).
Sokol, A.G., Palyanova, G.A., Palyanov, Y.N., Tomilenko, A.A., Melenevsky, V.N., 2009. Fluid regime and diamond formation in the reduced mantle: experimental constraints. Geochim. Cosmochim. Acta 73, 5820–5834.
Sokol, A.G., Tomilenko, A.A., Bul'bak, T.A., Palyanova, G.A., Sokol, I.A., Palyanov, Y.N., 2017. Carbon and nitrogen speciation in nitrogen-rich C-O–H–N fluids at 5.5–7.8GPa. Earth Planet. Sci. Lett. 460, 234–243.
Spetsius, Z.V., Cliff, J., Griffin, W.L., O'Reilly, S.Y., 2017. Carbon isotopes of eclogite-hosted diamonds from the Nyurbinskaya kimberlite pipe, Yakutia: the metasomatic origin of diamonds. Chem. Geol. 455, 131–147.
Spetsius, Z.V., Griffin, W.L., Taylor, L.A., O'Reilly, S.Y., Mityukhin, S.I., Valley, J.W., Spicuzza, M., 2008. Trace elements and oxygen isotopes in garnets from diamondiferous xenoliths, nurbinskaya pipe, Yakutia: implications for diamond genesis. 9th International Kimberlite Conference. Extended Abstract 9IKC-A-00140.
Stachel, T., Harris, J.W., 2009. Formation of diamond in the Earth's mantle. J. Phys.: Condens. Matter 21, 1–9.
Stachel, T., Luth, R.W., 2015. Diamond formation – Where, when and how? Lithos 220–223, 200–220.
Stagno, V., Ojwang, D.O., McCammon, C.A., Frost, D.J., 2013. The oxidation state of the mantle and the extraction of carbon from Earth's interior. Nature 493, 84–90.
Stagno, V., Frost, D.J., McCammon, C.A., Mohseni, H., Fei, Y., 2015. The oxygen fugacity at which graphite or diamond forms from carbonate-bearing melts in eclogitic rocks. Contrib. Miner. Petrol. 169, 16.
Sumiya, H., Toda, N., Satoh, S., 2002. Growth rate of high-quality large diamond crystals. J. Cryst. Growth 237–239, 1281–1285.
Takafuji, N., Hirose, K., 2005. Solubilities of O and Si in liquid iron in equilibrium with (Mg, Fe)Si_O3 perovskite and the light elements in the core. Geophys. Res. Lett. 32, L06313.
Tappert, R., Stachel, T., Harris, J.W., Muehlenbachs, K., Ludwig, T., Grey, G.P., 2005. Diamonds from Jagersfontein (South Africa): messengers from the sublithospheric mantle. Contrib. Miner. Petrol. 150, 505–522.
Taylor, L.A., Anand, M., Promprated, P., Floss, C., Sobolev, N.V., 2003. The significance of mineral inclusions in large diamonds from Yakutia, Russia. Am. Mineral. 88,

912–920.
Taylor, W.R., Green, D.H., 1989. The role of reduced C-O-H fluids in mantle partial melting. In: Ross, J.R. (Ed.), Proceedings of IVth International Kimberlite Conference. Special Publication-Geological society of Australia, vol. 14 (1), pp. 592–602.
Viljoen, K.S., Dobbe, R., Smit, B., 2009. Geochemical processes in peridotite xenoliths from the Premier diamond mine, South Africa: evidence for the depletion and re-feritilisation of subcratonic lithosphere. Lithos 112, 1133–1142.
Wood, B.J., 1991. Oxygen barometry of spinel peridotites. Rev. Mineral. Geochem. 25, 417–432.
Wyllie, P.J., Ryabchikov, I.D., 2000. Volatile components, magmas, and critical fluids in upwelling mantle. J. Petrol. 41, 1195–1206.
Zhang, C., Duan, Z.H., 2010. GFluid: an Excel spreadsheet for investigating C-O–H fluid composition under high temperatures and pressures. Computer Geosci. 36, 569–572.
Zhao, X.-Z., Rustum, R., Cherian, K.A., Badzian, A., 1997. Hydrothermal growth of diamond in metal–C–H_2O systems. Nature 385, 513–515.